Supporting Info

Real-time monitoring of a protein biomarker

Claudio Parolo,*[a] Andrea Idili,[a] Gabriel Ortega,[a] Andrew Csordas,[a] Alex Hsu,[a] Netzahualcóyotl Arroyo-Currás,[b] Qin Yang,[c] Brian Scott Ferguson,[c] Jinpeng Wang,[c] and Kevin W. Plaxco* [a], [d]

[a] Department of Chemistry and Biochemistry, University of California, Santa Barbara, Santa Barbara, CA 93106, United States

[b] Department of Pharmacology and Molecular Sciences, Johns Hopkins School of Medicine, Baltimore, MD 21205, United States

[c] Aptitude Medical Systems, Inc. Santa Barbara, CA 93105, United States

[d] Interdepartmental Program in Biomolecular Science and Engineering University of California, Santa Barbara, Santa Barbara, CA 93106, United States

Materials and methods

Materials

Unless otherwise stated we purchased all chemical reagents from Sigma-Aldrich (St. Louis, MO, USA). These include sodium hydroxide, sulfuric acid, 6-mercapto-1-hexanol, sodium chloride, ethanol, tris(2-carboxyethyl)-phosphine hydrochloride (TCEP), magnesium chloride, ethylenediaminetetraacetic acid (EDTA), potassium chloride, and sodium phosphate monobasic. We also employed artificial urine (Surine). The exact chemical composition of this widely used,[1,2] certified reference material (accepted for use in LC/MS or GC/MS applications for clinical chemistry, urine drug testing or forensic analysis) is not available.

We purchased HPLC-purified oligonucleotides from Biosearch Technologies (Novato, CA, USA). These (Table 1S) were modified with a thiol-C6-SS group on the 3′ end, and a methylene blue on the 5′ end. We then dissolved them in ultra-pure water at a concentration of 100 μM and stored at -20 °C. We determined the oligonucleotide concentration measuring the absorbance at 260 nm using a Beckman Coulter DU 800 UV-Vis spectrophotometer (Männedorf, Switzerland).

Table 1S: Sequences of the aptamer truncations.

Name	Sequence
Full Length	SH-5'-GAATTCCGCCCTCGTCCCATCTC **GGCTTGGTATGGCGGAGCTGGATAGTATAGTCGG** AACACCAACCGAGAACGGAATTC-3'-MB
5'primer-truncated	SH-5'-**GGCTTGGTATGGCGGAGCTGGATAGTATAGTCGG** AACACCAACCGAGAACGGAATTC-3'- MB
3'primer-truncated	SH-5'-GAATTCCGCCCTCGTCCCATCTC **GGCTTGGTATGGCGGAGCTGGATAGTATAGTCGG**-3'-MB
34-base (primer-less)	SH-5'-**GGCTTGGTATGGCGGAGCTGGATAGTATAGTCGG**-3'-MB
30-base	SH-5'- **TGGTATGGCGGAGCTGGATAGTATAGTCGG**-3'-MB
26-base	SH-5'- **ATGGCGGAGCTGGATAGTATAGTCGG**-3'-MB
22-base	SH-5'- **CGGAGCTGGATAGTATAGTCGG**-3'-MB

The underlined bases correspond to the primer sequences used during the aptamer selection. The bold sequences correspond to the core region that is thought to bind the target.

EAB sensor fabrication using gold macro-electrodes

First we manually polished rod gold disk electrodes (3.0-mm diameter, BAS, West Lafayette, IN, USA) first using a microcloth pad soaked with 1-μm diamond suspension slurry and then with a 0.05-μm alumina powder aqueous suspension (both purchased by MetaDi, Buehler, Lake Bluff, IL, USA). After each polishing step we sonicated the electrodes in a solution of 1:1 water/ethanol for 5 min. Then we further cleaned the electrodes by: 1) performing 1000–2000 scans of cyclic voltammetry in a 0.5 M NaOH solution using a potential between -0.4 and -1.35 V (this and all other potentials versus Ag/AgCl) at a scan rate of 2 V s^{-1}; 2) applying an oxidizing potential of 2 V for 5 s in 0.5 M H_2SO_4 solution; 3) applying a reducing potential of -0.35 V for 10 s in 0.5 M H_2SO_4 solution; and, finally, 4) performing 10 scans of cyclic voltammetry in 0.5 M H_2SO_4 solution using a potential between -0.35 and 1.5 V at 4 V s^{-1}.

We next reduced a solution of 16 μM of aptamer in 10 mM TCEP in the dark for 1 h before then diluting this to 500 nM aptamer using PBS. We then incubated clean electrodes in this solution for 1 h at room temperature in the dark. After rinsing the electrode surface with milliQ water we incubated each in 20 mM 6-mercaptohexanol over night at 4 °C. Before employing the sensor we further rinsed each electrode with milliQ water.

We performed the electrochemical measurements using a CHI660D potentiostat with a CHI684 Multiplexer (CH Instruments, Austin, TX) and a standard three-electrode cell containing a platinum counter electrode and a Ag/AgCl (3 M KCl) reference electrode (CH Instruments, Austin, TX). We carried out square wave voltammetry (SWV) using a potential window of -0.05 to -0.45 V, a potential step of 0.001 V, and an amplitude of 0.05 V.

EAB sensor fabrication using micro-electrodes

The EAB sensors employed for the real-time measurement of NGAL (Figure 3) were fabricated following previous reports.[3,4] Briefly, segments of pure gold (7.75 cm in length), platinum (7.25 cm), and silver (6.75 cm) wire were cut and approximately 1 cm of insulation was removed using a surgical blade to allow electrical contact. The wires were then soldered each to one of the three ends of a connector cable using 60% tin/40% lead rosin-core solder (0.8 mm diameter) and bound together by applying heat to shrinkable tubing around the body of the wires, except for a small window (~ 5 mm) at the end of each wire. The wires were attached in a layered fashion, with the gold wire being insulated alone first, then both gold and platinum wires together, and finally all three wires together. The purpose of this three-layer-thick insulation was to give mechanical strength to the body of the malleable probe. To prevent electrical shorts between wires, different lengths were used for each wire as described above. The sensor window (i.e., the region devoid of insulation) in the gold wire was cut to approximately 3 mm in length. The EAB sensors employed for the calibration curve (Figure S3) were fabricated using only a segment of pure gold (7.75 cm in length) wire and the same

previous described protocol. During the electrochemical measurements an external platinum counter electrode and a Ag/AgCl (3 M KCl) reference electrode (CH Instruments, Austin, TX) were used. To increase the surface area of the gold working electrodes (to obtain larger peak currents) the sensor surface was roughened electrochemically via immersion in 0.5 M sulfuric acid followed by stepping the potential back and forth from $E_{initial}$ = 0.0 V to E_{high} = 2.0 V, for 16 000 pulses.[3] Each potential step was of 20 ms duration with no wait time between pulses. We then deposited aptamer on the sensor as descried above.

Artificial bladder experiments

To simulate a clinical scenario in which NGAL is slowly released into urine we constructed an artificial bladder consisting of a medical grade, sterile 14fr Foley catheter inserted through the drain (mimicking the urethra) of a 250 mL bag of saline (mimicking the bladder). Synthetic urine from this artificial bladder flowed down the catheter driven by gravitational force. Because we were interested in performing EAB measurements for hours, we placed the catheter drain inside a receiving 500 mL beaker that, in turn, contained the inlet line of a gear pump (Benchtop Analog Drive, 0.261 mL/rev) from Cole Parmer (Vernon Hills, IL). The pump outlet was connected to a second port in the saline bag. We adjusted the revolutions of this pump so that, when turned on, it brought synthetic urine from the beaker into the bag at the same rate as the liquid was driven down the catheter by gravitational force. The artificial bladder never contained more than 100 mL of synthetic urine in the system (beaker, catheter, pump, and bag). This setup allowed us to continuously recirculate the synthetic urine for hours. To emulate NGAL release, we placed a drug line from a syringe pump (Cetoni NemeSys, Germany) into the receiving beaker, and performed a constant-rate infusion of an NGAL stock solution in synthetic urine, with a rate adjusted to achieve a final concentration of NGAL in the artificial bladder of 32 nM in 1 h. Our EAB sensors were inserted into the downstream catheter through the sidewalls, tightly sealed in place with Parafilm and had no leaks. We serially interrogated our EAB sensors by square wave voltammetry at different frequencies and analyzed the so produced voltammograms both in real time and during postprocessing using SACMES, a previously published custom Python script developed by our labs.[5]

NGAL expression and purification

We obtained a plasmid containing the gene encoding NGAL from Aptitude (Santa Barbara, CA). The gene is cloned into an ampicillin-resistant pET-21a plasmid between the restriction sites Nde I and Xho I, thus incorporating a hexa-histidine tag at its C-terminus (NGAL amino acid sequence is as follows:

MTSDLIPAPPLSKVPLQQNFQDNQFQGKWYVVGLAGNAILREDKDPQKMYATIYEL
KEDKSYNVTSVLFRKKKCDYWIRTFVPGSQPGEFTLGNIKSYPGLTSYLVRVVSTNY
NQHAMVFFKKVSQNREYFKITLYGRTKELTSELKENFIRFSKSLGLPENHIVFPVPIDQ
CIDGLEHHHHHH.

To obtain the protein we transformed the plasmid into *E. coli* BL21(DE3) cells (New England Biolabs, Ipswich, MA), and then induced expression using 1 mM IPTG for 1 h at 37 ºC. After cell lysis we performed His-tag affinity chromatography (HisTrap HP-5mL, GE Healthcare,

Chicago, IL) and size exclusion chromatography (Superdex S100, GE Healthcare, Chicago, IL) in buffer 50 mM sodium phosphate (pH = 7.0) and 100 mM sodium chloride. We then used UV-Vis spectroscopy to assess protein concentration (molar absorption coefficient at 280 nm was 26,025 M^{-1} cm^{-1}). Typical overexpression and purification yields were in the order of 50 mg per liter of culture.

EAB sensor optimization

We challenged sensors fabricated using each of the seven aptamer truncations with increasing concentrations of NGAL over the range 300 pM to 1 µM. The full length 80-base aptamer failed in producing a detectable methylene blue peak at any of the concentrations. The next two shorter variants (5`-primer truncated and 3`-primer truncated) produced a lower signal change compared to the shortest versions. Looking at the four shortest variants, the 22-base produced the smallest signal change (20%) and the highest Kd (396 nM). The 34-base and 30-base versions exhibited similar maximum signal changes (~ 30%), but with the 30-base having a improved Kd (86 nM vs 224 nM). The 26-base aptamer, in contrast, produced a larger signal change (100%) and the second lowest Kd (185 nM). Given this we selected the 26-base to serve as the recognition element in the EAB sensor described here.

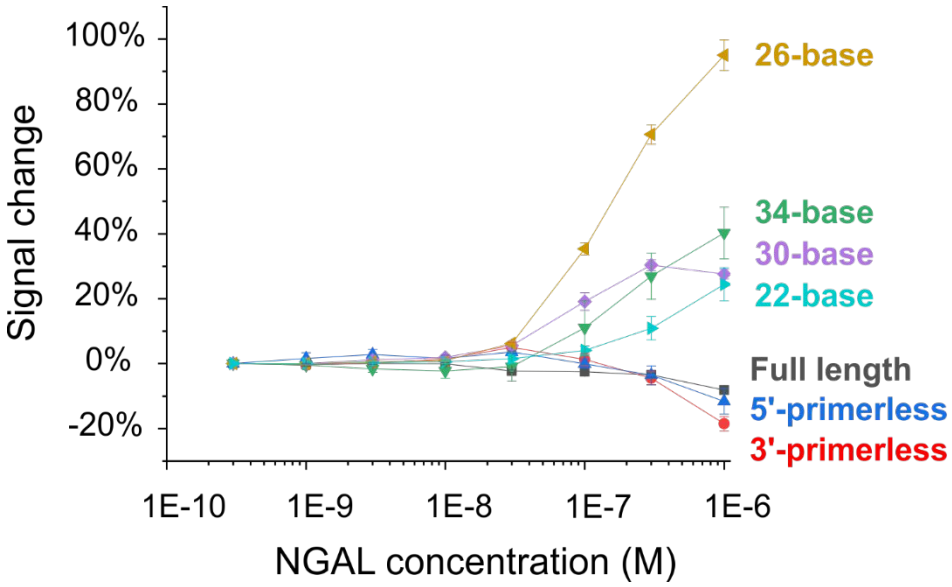

Figure 1S: Calibration curves obtained using the seven different aptamer variants. The 26-base variant provides the highest signal gain, and thus we employed it in our work.

Analysis of authentic urine using a commercial ELISA

To determine the baseline level of NGAL present in healthy urine we employed a commercial ELISA kit (Human Lipocalin-2/NGAL Quantikine ELISA Kit, Minneapolis, MN). The resulting concentration, 156 pM, is two orders of magnitude lower than the lower end of the useful dynamic range of the EAB sensor response. This value is also an order of magnitude lower than the lowest clinically relevant cut-off threshold (2 nM).

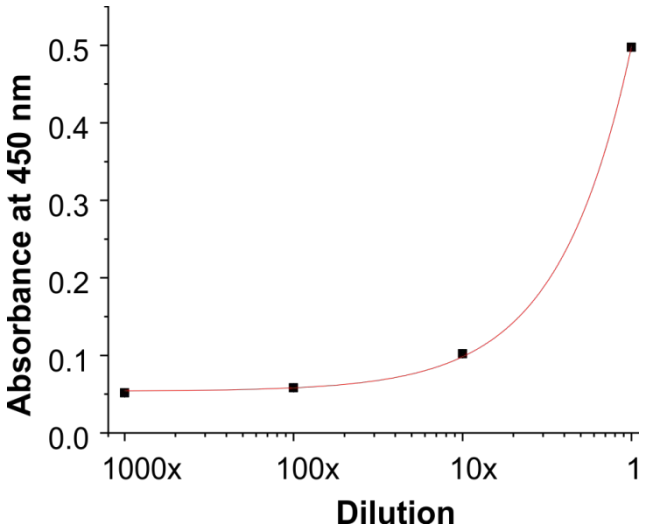

Figure 2S: A calibration curve obtained diluting authentic urine sample following the protocol specified by the Human Lipocalin-2/NGAL Quantikine ELISA Kit. The resulting concentration, 156 pM, is far below the lowest reported clinical cutoff and two orders of magnitude lower than the dynamic range of the EAB response. The linear fitting equation correspond to $y = 0.054 + 0.445[NGAL]$ and has an R^2 of 0.999.

EAB sensor specificity

We proved the EAB sensor selectivity by spiking three different proteins at a concentration in the range of NGAL clinical cutoffs. None of these produced any significant signal change (Fig. 3S).

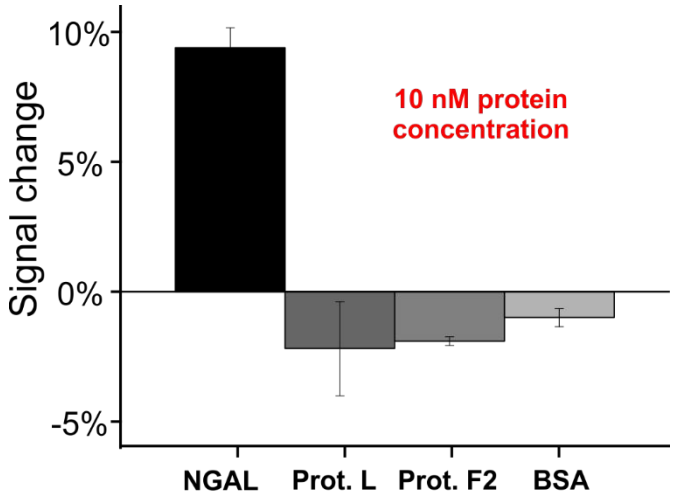

Figure 3S: The EAB sensor responded to 10 nM of NGAL producing a +10% signal change, while the addition of 10 nM of protein L, thrombin (F2) and bovine serum albumin (BSA) produced approximately -2% signal change. The bars and error bars represent the average and standard deviations of three independently fabricated sensors.

Microelectrode calibration

To quantify the measurements made using the sensors inside the urinary catheter, we also determined a calibration curve for EAB sensors fabricated gold microelectrodes. Their response is similar to that obtained using macro electrodes and follows the expected Langmuir Isotherm model, producing a dynamic range spanning approximately between 10 nM and 810 nM (representing the transition from 10% to 90% site occupancy).

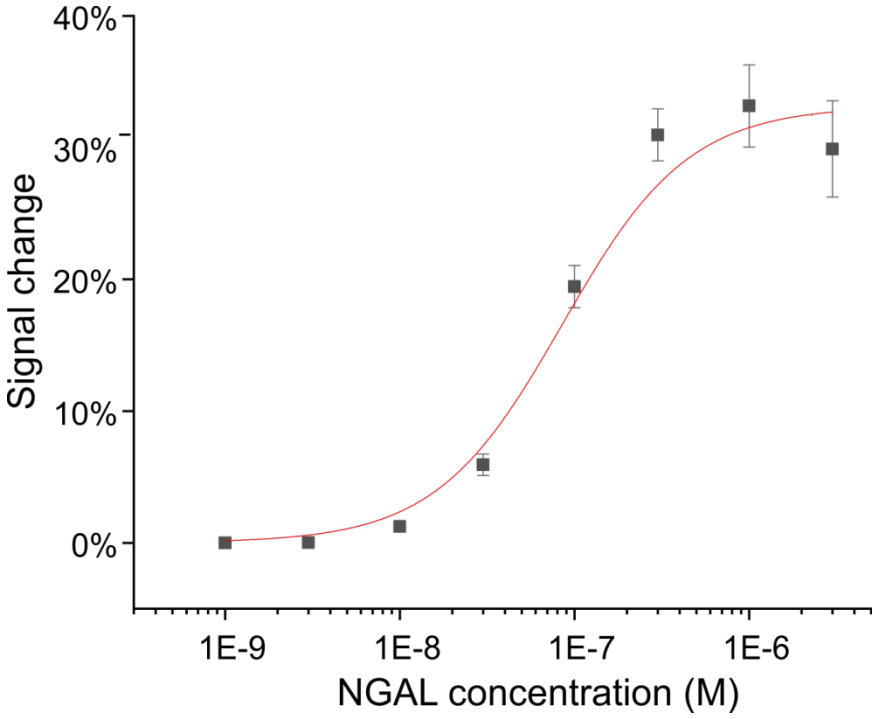

Figure 4S: Calibration curve obtained using the gold microelectrodes we employed inside the urinary catheter. The data represent the average and standard deviations of at least three independently fabricated sensors.

Packing density effects

The density with which aptamers are on the electrode surface is a key aspect to optimize during the development of an EAB sensor. Specifically, lower packing density is often associated with higher affinity,[6] but also often produces reduced signalling current and lower signal gain. For this EAB sensor we observe that using deposition concentrations of 500 nM produced a K_d of 121 nM and gain of 100%. A deposition concentration of 25 nM, in contrast, produced a K_d of 58 nM and gain of 40%.

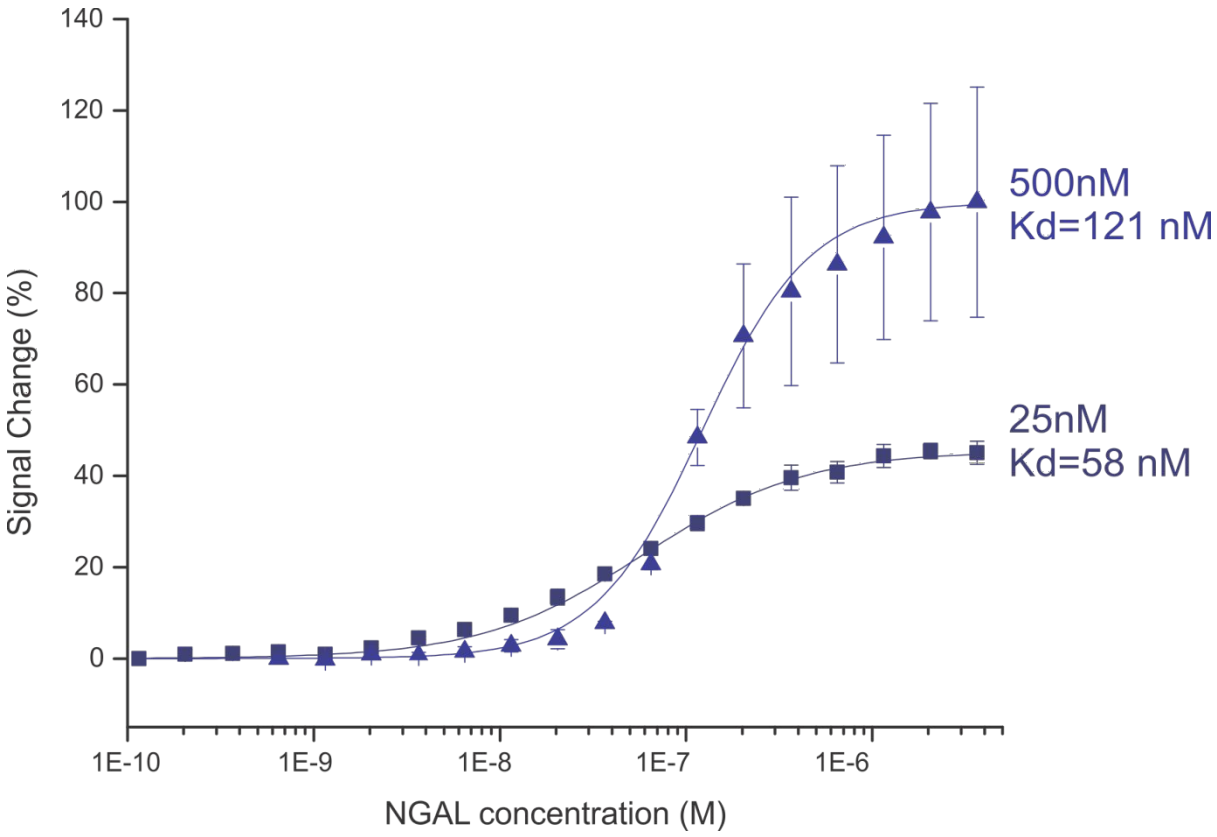

Figure 5S: Calibration curves obtained using sensors fabricated using different deposition concentrations of the 26-base variant. While lower deposition concentrations produce better affinity, higher deposition concentrations improve signal gain.

Bibliography

(1) Rees, M.; Wright, A. G.; Holdcroft, S.; Bertoncello, P. Voltammetry at Hexamethyl-P-Terphenyl Poly(Benzimidazolium) (HMT-PMBI)-Coated Glassy Carbon Electrodes: Charge Transport Properties and Detection of Uric and Ascorbic Acid. *Sensors* **2020**, *20* (2), 443. https://doi.org/10.3390/s20020443.

(2) McCulloch, R. D.; Robb, D. B. Field-Free Atmospheric Pressure Photoionization–Liquid Chromatography–Mass Spectrometry for the Analysis of Steroids within Complex Biological Matrices. *Anal. Chem.* **2017**, *89* (7), 4169–4176. https://doi.org/10.1021/acs.analchem.7b00157.

(3) Arroyo-Currás, N.; Scida, K.; Ploense, K. L.; Kippin, T. E.; Plaxco, K. W. High Surface Area Electrodes Generated via Electrochemical Roughening Improve the Signaling of Electrochemical Aptamer-Based Biosensors. *Anal. Chem.* **2017**, *89* (22), 12185–12191. https://doi.org/10.1021/acs.analchem.7b02830.

(4) Idili, A.; Arroyo-Currás, N.; Ploense, K. L.; Csordas, A. T.; Kuwahara, M.; Kippin, T. E.; Plaxco, K. W. Seconds-Resolved Pharmacokinetic Measurements of the Chemotherapeutic Irinotecan in Situ in the Living Body. *Chem. Sci.* **2019**, *10* (35), 8164–8170. https://doi.org/10.1039/c9sc01495k.

(5) Curtis, S. D.; Ploense, K. L.; Kurnik, M.; Ortega, G.; Parolo, C.; Kippin, T. E.; Plaxco, K. W.; Arroyo-Currás, N. Open Source Software for the Real-Time Control, Processing, and Visualization of High-Volume Electrochemical Data. *Anal. Chem.* **2019**, *91* (19), 12321–12328. https://doi.org/10.1021/acs.analchem.9b02553.

(6) Esteban Fernández de Ávila, B.; Watkins, H. M.; Pingarrón, J. M.; Plaxco, K. W.; Palleschi, G.; Ricci, F. Determinants of the Detection Limit and Specificity of Surface-Based Biosensors. *Anal. Chem.* **2013**, *85* (14), 6593–6597. https://doi.org/10.1021/ac4012123.